Spatter Tracking in Laser Machining

Timo Viitanen, Jari Kolehmainen, Robert Piché, and Yasuhiro Okamoto

Abstract. In laser drilling, an assist gas is often used to remove material from the drilling point. In order to design assist gas nozzles to minimize spatter formation, measurements of spatter trajectories are required.
We apply computer vision methods to measure the 3D trajectories of spatter particles in a laser cutting event using a stereo camera configuration. We also propose a novel method for calibration of a weak perspective camera that is effective in our application.
The proposed method is evaluated with both computer-generated video and video taken from actual laser drilling events. The method performs well on different workpiece materials.

1 Introduction

In laser drilling, a laser beam is focused on a workpiece to melt or vaporize the material, forming a hole. Often a jet of high-speed assist gas is applied to blow molten material away from the hole. A recent advance in the field is the use of a Laval nozzle whose shape accelerates the gas to supersonic speed [1].

A common defect associated with laser drilling is that some material ejected from the hole lands back on the workpiece and resolidifies, forming spatter. An example of spatter is shown in Figure 1a. This is especially undesirable in applications that require high precision. There is therefore interest in improving the design of an assist gas nozzle to minimize spatter formation. For example, the material could be expelled away from the workpiece, or caught at a shield. To guide the designer, the motion of spatter particles can be predicted with CFD simulation. However, measurements are needed to calibrate the simulation models and to verify the models' fidelity.

The objective of this study is to analyze video of laser drilling events taken with a stereo configuration of two high-speed cameras. An example video frame is shown in Figure 1b. This study is structured as follows. First we discuss calibration of such a camera configuration, and propose a method for calibration of a weak perspective camera that is effective for this application. We then apply a sequential Monte Carlo (SMC) filter to track spatter particles in the video. We pair tracks using the epipolar constraint and perform 3D reconstruction using an unscented Kalman filter (UKF). Finally, we evaluate the proposed method with synthetic video, and video taken from 30 laser drilling events. Results reported in [2] were computed using this method.

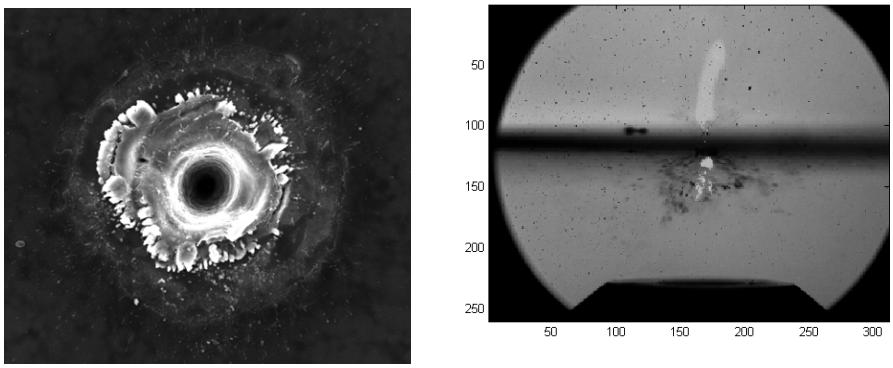

(a) Spatter formation surrounding a laser drilled hole.

(b) A typical input video frame.

Fig. 1: Laser drilling

2 Camera calibration

2.1 Overview

A main obstacle in this study was obtaining accurate calibration. We initially attempted calibration with Zhang's method [3]. However, the results obtained this way suffered from a large reprojection error. We found that Zhang's method is unsuitable for an application such as ours, where observations are noisy and cameras are close to affine, and developed a method based on the weak perspective camera model.

Like Zhang's method, our method requires images of a calibration object. A sample calibration image is shown in Figure 2d. We first calculate homography matrices, which relate the model plane to each image. Using these matrices, we estimate the intrinsic parameters that are common to all images. We then solve the extrinsic parameters that describe the calibration object's position and orientation in each image. The following sections describe these steps in more detail. [3]

2.2 Weak perspective camera model

The affine camera is an abstract model of a camera whose focal length is very large compared to the object being viewed. The model is accurate for e.g. microscopes. An affine camera constrained to have zero skew is called a *weak perspective camera*. Compared to the projective camera, which has 5 intrinsic and 6 extrinsic parameters, a weak perspective camera has 2 and 5 respectively, making it more analytically tractable.

The cameras used in our study have a focal length of tens of centimeters, and our calibration object is 1 mm wide, making them practically indistinguishable from affine cameras.

Let $x \in \mathbb{R}^2$ be a point in the image plane and $z \in \mathbb{R}^3$ be a point in space. An affine camera model is given by

$$x = \mathrm{M}z + t. \tag{1}$$

where M is a 2×3 matrix and t is a translation vector. Using homogenous coordinates, the affine camera model can be written as

$$\begin{bmatrix} x \\ 1 \end{bmatrix} = \mathrm{P} \begin{bmatrix} z \\ 1 \end{bmatrix}, \tag{2}$$

$$\mathrm{P} = \begin{bmatrix} M_{11} & M_{12} & M_{13} & t_1 \\ M_{21} & M_{22} & M_{23} & t_2 \\ 0 & 0 & 0 & 1 \end{bmatrix}. \tag{3}$$

The matrix M can be decomposed as $\mathrm{M} = \mathrm{A}_{22}\mathrm{R}_{1:2,1:3}$, where A_{22} is an affine calibration matrix and $\mathrm{R}_{1:2,1:3}$ consists of the first two rows of a rotation matrix. The calibration matrix is of the form

$$\mathrm{A}_{22} = \begin{bmatrix} \alpha & 0 \\ \gamma & \beta \end{bmatrix} = \begin{bmatrix} \alpha & 0 \\ 0 & \beta \end{bmatrix}. \tag{4}$$

where α and β represent focal length and aspect ratio, and γ the skew of the camera, which we constrain to be 0.

2.3 Homography

An affine mapping from a 3D plane to an image plane can be represented by an affine homography matrix $\mathrm{H} \in \mathbb{R}^{3\times3}$ whose last row is $[0, 0, 1]$. Without loss of generality we can choose a coordinate system such that the image plane lies in xy-plane, so that z equals zero. We can then write the homography in terms of the projection matrix:

$$H = \begin{bmatrix} M_{11} & M_{12} & t_1 \\ M_{21} & M_{22} & t_2 \\ 0 & 0 & 1 \end{bmatrix}. \tag{5}$$

2.4 Solving for focal length and aspect ratio

Given a set of homographies $\{\mathrm{H}^{(k)}\}$, the objective of affine calibration is to find the calibration matrix A, rotation matrices $\{\mathrm{R}^{(k)}\}$ and translation vectors $\{t^{(k)}\}$ that fit the given homographies.

First of all we denote $\mathrm{A}_{ii} = \alpha_i$. Now from the first two colums of the homography H we obtain two equations

$$h^{(i)}_{1:2} = \alpha_i r^{(i)}_{1:2}, \text{ for } i \in \{1, 2\}. \tag{6}$$

Adding the missing rotation components, Equation (6) becomes

$$[h_{1:2}^{(i)}, \alpha_i r_3^{(i)}]^{\mathrm{T}} = \alpha_i r^{(i)}. \tag{7}$$

Knowing that $\|r^{(i)}\| = 1$, and that $r^{(1)} \cdot r^{(2)} = 0$ we obtain three equations

$$\left(r_3^{(i)}\right)^2 = \frac{\|h_{1:2}^{(i)}\|^2 - \alpha_i^2}{\alpha_i^2}, \text{ for } i \in \{1, 2\}, \text{ and} \tag{8}$$

$$h_{1:2}^{(1)} \cdot h_{1:2}^{(2)} = -\alpha_1 \alpha_2 r_3^{(1)} r_3^{(2)}. \tag{9}$$

Eliminating rotation elements $r_3^{(i)}$ yields

$$\left(h_{1:2}^{(1)} \cdot h_{1:2}^{(2)}\right)^2 - \|h_{1:2}^{(1)}\|^2 \|h_{1:2}^{(2)}\|^2 = -\|h_{1:2}^{(2)}\|^2 \alpha_1^2 - \|h_{1:2}^{(1)}\|^2 \alpha_2^2 + (\alpha_1 \alpha_2)^2. \tag{10}$$

Denoting the expression on the left of (10) as b_k, where k denotes the index of homography used, and $a_k = -[\|\|h_{1:2}^{(2)}\|^2, h_{1:2}^{(1)}\|^2]^{\mathrm{T}}$, we obtain

$$b_k = a_k [\alpha_1^2, \alpha_2^2]^{\mathrm{T}} + (\alpha_1 \alpha_2)^2. \tag{11}$$

Taking the differences of any two equations with different indices yields

$$b_{k_1} - b_{k_2} = (a_{k_1} - a_{k_2}) [\alpha_1^2, \alpha_2^2]^{\mathrm{T}}. \tag{12}$$

For a set of n images, (12) determines an overdetermined set of $O(n^2)$ linear equations to be solved in the least-squares sense.

2.5 Solving for rotation and translation

Due to the affine nature of the problem, translation is equal to the last column of homography (if it is scaled so that $\mathrm{H}_{33} = 1$), that is,

$$t = h^{(3)}. \tag{13}$$

We can obtain the top left 2×2 block of the rotation matrix as

$$r_{1:2}^{(i)} = \alpha_i^{-1} h_{1:2}^{(i)}. \tag{14}$$

Now we need to find a rotation matrix that fits the 2×2 block. The last component of a column can be obtained from the unity constraint as

$$r_3^{(i)} = \pm \sqrt{1 - \min(1, \|r_{1:2}^{(i)}\|^2)}, \tag{15}$$

where the minimum is added to ensure numerical stability. Signs are chosen so that they preserve orthogonality and right-handedness. The last row is obtained using the well-known relationship [3]

$$r^{(3)} = r^{(1)} \times r^{(2)}, \tag{16}$$

After invoking Equation (15), the full rotation matrix is adjusted using SVD-decomposition to ensure its orthogonality. This procedure also eliminates mirroring.

The parameters obtained in this way could be used as an initial guess for further optimization that minimizes the reprojection error, as in [3], but this was not done in this study.

2.6 Evaluation

We compared our method to Zhang's using simulated data. In each trial, we performed camera calibration with ten synthetic views of a calibration object, taken at equal distance from random directions, perturbed with Gaussian noise. We varied the distance and the mean deviation of the noise, ran 100 trials for every parameter pair, and compared the reprojection RMSE statistic for each method. The results are shown in Figure 2.

With zero noise, Zhang's method outperforms ours at any distance, since it solves the original camera matrix, which is not exactly affine. Also, near the calibration object, the affine camera is a poor approximation and this causes large errors for our method. Further away, Zhang's method becomes highly susceptible to small amounts of noise, while our method remains robust. In our application the noise std. dev. is of order 10^{-3} in normalized coordinates and the distance is approximately 10^3. As seen in Figure 2, these conditions are very suitable for our method and unsuitable for Zhang's.

3 Spatter object tracking

3.1 SMC filter

Sequential Monte Carlo (SMC) filtering is a method used to estimate the state of a discrete-time nonlinear dynamic system. It is applied on similar problems for instance in [4]. A dynamic system has a state sequence x_k and a measurement sequence y_k. The state's evolution is specified by a probabilistic model given by[1]

$$x_k|x_{k-1} \sim p(x_k|x_{k-1}). \tag{17}$$

The state x_k is connected to the measurement y_k by the observation model given by

$$y_k|x_k \sim p(y_k|x_k) \propto L(y_k|x_k), \tag{18}$$

where $L(y|x_k)$ is called likelihood. Likelihood needs only be known up to a multiplicative constant. The solution of the problem is the posterior density $p(x_k|y_{1:k})$. In this study, the state is the position of a spatter object. We used the SIFT method to detect candidate spatter particles in the video [5].

[1] For the sake of notational simplicity, the distinction between random variables and their realized values (e.g. using bold font or upper case) is not made.

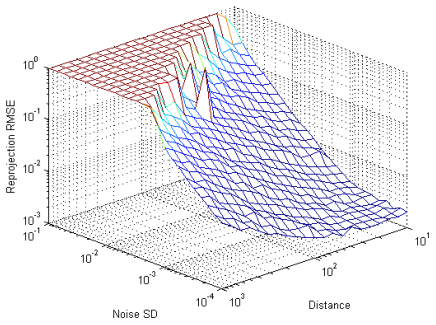

(a) Error analysis of Zhang's method. The method is at its best close to the calibration object, and quickly becomes susceptible to noise as distance grows. The RMSE is capped at 0.1 for clarity, but it may rise up to 10^6.

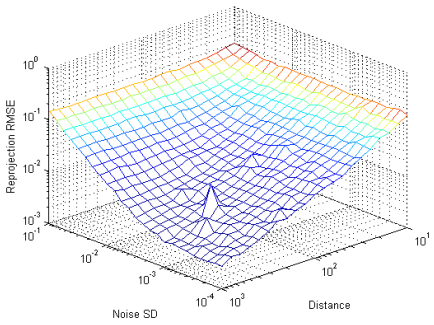

(b) Error analysis of the affine method. At close distance the affine approximation is unusable. The method grows more accurate as distance grows. With very high noise, the results are less erratic than in Zhang's but still useless.

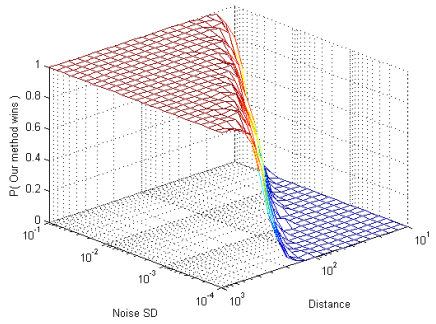

(c) Comparison of the affine method to Zhang's. The Z-axis represents the proportion of trial runs where our method had the lower RMSE.

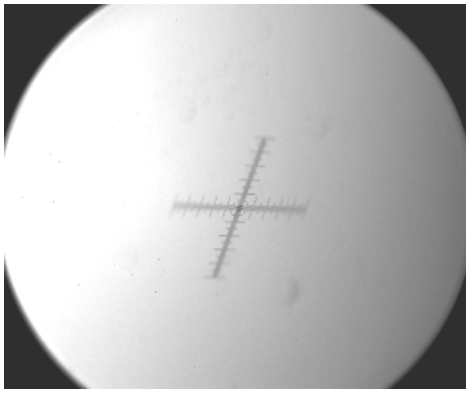

(d) A typical calibration image.

Fig. 2: Evaluation of the proposed affine calibration method with synthetic data. The calibration object is 10 units wide. The noise is added to normalized image coordinates that range between $-1..1$.

A SMC filter solves the problem by approximating the posterior density with set of N samples $\{x_k^{(i)}\}$ and associated weights $\{w_k^{(i)}\}$ by Equation (19)

$$p(x_k|y_{1:k}) \approx \sum_{i \leq N} w_k^{(i)} \delta(x_k - x_k^{(i)}). \tag{19}$$

Samples are drawn from the distribution $\pi(x_k|x_{1:k-1}, y_{1:k})$, which is called the proposal distribution. [6]

3.2 State evolution model

The state evolution model in this study embodies the assumption that the velocity of a spatter particle does not change much in one time step. We estimate velocity as

$$v_k = x_k - x_{k-1}. \tag{20}$$

which yields the following state model,

$$x_k = x_{k-1} + v_{k-1} + \varepsilon_k = 2x_{k-1} - x_{k-2} + \varepsilon_k, \tag{21}$$

where ε_k is a normally distributed error term.

3.3 Observation model

In a laser drilling video, spatter objects are observed as dark dots relative to background. The user specifies a background color b_k and a threshold $\theta \geq 0$.

Let $I_k(x)$ be the intensity at the image point x at time k. Likelihood was computed in a neighborhood U_x of the point x. Mean intensity in a neighborhood U_x is given by Equation (22)

$$\overline{I}_k(x) = \frac{\int_{U_x} I(x^{'})dx^{'}}{\int_{U_x} dx^{'}}. \tag{22}$$

In the discrete case integrals are treated as sums. Three criteria were used to formulate a likelihood function that recognizes particles. Particles should be distinct from background color, and the mean intensity and texture of a particle should remain similar in consecutive frames. The likelihood used in this study is given by

$$\begin{aligned} L(I|x_{1:k}, I_{k-1}) = {} & \left(\overline{I}(x_k) - b_k\right)^2 H\left(\left(\overline{I}(x_k) - b_k\right)^2 - \theta\right) \times \\ & \exp\left(-\frac{1}{2}\frac{\left(\overline{I}(x_k) - \overline{I}_{k-1}(x_{k-1}\right)^2}{\sigma_I \max(I)^2}\right) \times \\ & \int_{U_0} \exp\left(-\frac{1}{2}\frac{\left(I(x^{'} + x_k) - I_{k-1}(x^{'} + x_{k-1})\right)^2}{\sigma_I \max(I)^2}\right) dx^{'} \end{aligned} \tag{23}$$

where σ_I denotes the assumed intensity covariance of points in consecutive frames and $H(\cdot)$ is the Heaviside function. In this study a square neighborhood of 5×5 pixels was used. An ellipse was also tested, but it gave no noticeable advantage over the square.

3.4 Proposal distribution

In SMC filtering it is common to use bootstrap filtering, where the state model is the proposal distribution for the sampling. However in a spatter tracking application particles are small and bootstrap filtering leads to sampling from regions that are of no interest. To make tracking more efficient, we used data dependent sampling, where part of the likelihood is merged to the proposal distribution [4]. This lead to a proposal distribution given by

$$\pi(x_k|x_{1:k-1}, I_{1:k}) \propto p_{x_k|x_{k-1}}(x_k|x_{k-1}) \exp\left(-\frac{1}{2}\frac{\left(\overline{I}_k(x_k) - \overline{I}_{k-1}(x_{k-1})\right)^2}{\sigma_I \max(I_k)^2}\right). \tag{24}$$

Sampling from this proposal distribution can be achieved using Metropolis-Hastings algorithm [7] with the state model $p_{x_k|x_{k-1}}(x_k|x_{k-1})$ as a target distribution. This caused most samples to end up inside a spatter particle, allowing the use of very small sample sizes. We achieved good performance with a short random walk of tens of samples.

4 3D reconstruction

4.1 Spatter object matching

After tracking spatter objects in the separate videos from the two cameras, we match them to form pairs. Image points $x, x^{'} \in \mathbb{P}^2$ from different views must satisfy the equation

$$x^T \mathrm{F} x' = 0, \tag{25}$$

where F is the fundamental matrix between the two views. The fundamental matrix can be computed from 7 point correspondences between two images. [8]

We matched each particle to the particle that minimizes the mean of $x^T \mathrm{F} x'$ over the shared lifetime of the pair. Since the fundamental matrix constrains the particles only to a line, not a point, this may result in spurious matches. To reduce the number of spurious matches, we reject very short tracks, as well as tracks that have a high reprojection error after reconstruction.

4.2 3D path reconstruction

In this study, 3D reconstruction was done by an unscented Kalman filter (UKF) [9]. The UKF solves problems similar to the SMC filter. Here the 2D locations of

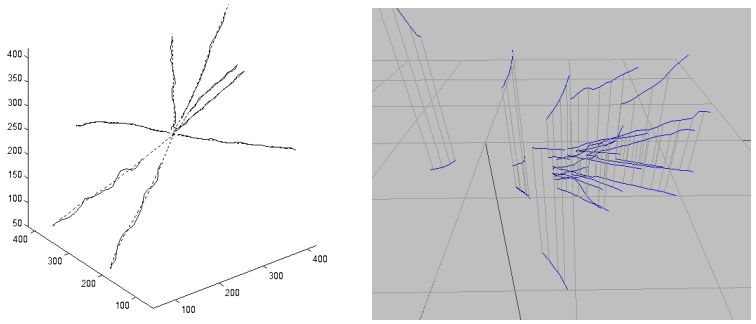

(a) Reconstruction from a synthetic test video with Matlab prototype. Dashed line: ground truth, Cont. line: reconstructed.

(b) Reconstruction from laser drilling data with a threaded C++ implementation.

Fig. 3: Evaluation

a particle were chosen as measurements and the state evolution model was similar to the one used with the SMC filter. An advantage of UKF over the extended Kalman filter (EKF) is that it doesn not require the computation of Jacobian matrices of these models. The standard constant velocity motion model[10] was used as the state evolution model.

Given camera matrices P_x and P_y of both cameras, the 3D position $z \in \mathbb{R}^3$ is connected to homogenous image coordinates x and y by

$$\begin{bmatrix} x \\ y \end{bmatrix} \propto \begin{bmatrix} \mathrm{P}_x \\ \mathrm{P}_y \end{bmatrix} z. \tag{26}$$

With a perspective camera, the observation model would be nonlinear due to the use of homogenous coordinates.

5 Evaluation of method

The proposed method was used to track particles in computer generated video and in actual laser drilling data. Tests with synthetic data showed that the method was accurate at least in conditions of constant lighting and low noise. Typical results from an eight particle test video are shown in Figure 3a.

The method was also tested on data measured from actual laser drilling events. The used laser was a Nd:YAG-laser, with a pulse energy of 0.2 J. 30 videos were recorded. Each video recorded a single laser pulse applied to a workpiece. The assist gas was nitrogen, with cylinder pressure 0.6 MPa. Frame rate was 1 Mfps and exposure time was 0.5 µs.

Tests carried out with real data gave natural looking results. Typical results of spatter tracking can be seen in Figure 3b. Fuirther experimental results using the proposed tracking method are reported in [2].

6 Conclusions

The proposed method for spatter measurements produces plausible trajectory reconstructions from real data recorded by the high speed video cameras and obtains good accuracy in our simulated test cases. There is currently no other way to obtain detailed knowledge such as individual particle velocities or particle sizes for statistical analysis from a cutting event. The results will be used to calibrate and verify CFD simulation in assist gas nozzle design.

The method could also be used for spatter tracking in laser cutting of materials such as steel, aluminium and plastics. The main limitation is the use of oxygen as an assist gas, as it makes the observation of particles difficult.

Practical problems with the method were mostly associated with difficulty of obtaining accurate camera calibration. These problems were resolved by developing the weak-perspective calibration method described earlier. The weak perspective method may be useful for other applications, for example some Augmented Reality research uses Zhang's method to locate fiducial markers, for instance in [11]. Since markers may be relatively far from the camera, our method may be more robust.

References

1. Okamoto, Y., Uno, Y., Suzuki, H.: Effect of nozzle shape on micro-cutting performance of thin metal sheet by pulsed Nd: YAG laser. International Journal of Automation Technology **4** (2010)
2. Kolehmainen, J.T., Okamoto, Y., Yamamoto, H., Okada, A., Viitanen, T.T.: Measurement of the spatter velocity in fine laser cutting. International journal of Japan Society for Precision Engineering (2012)
3. Zhang, Z.: A flexible new technique for camera calibration. IEEE Trans. Pattern Anal. Mach. Intell. **22** (2000) 1330–1334
4. Smal, I., Niessen, W., Meijering, E.: Advanced particle filtering for multiple object tracking in dynamic fluorescence microscopy images. Biomedical Imaging: From Nano to Macro **4** (2007) 1048–1051
5. Lowe, D.: Object recognition from local scale-invariant features. Computer Vision **7** (1999) 1150–1157
6. Doucet, A., Godsill, S., Andrieu, C.: On sequential Monte Carlo sampling methods for Bayesian filtering. Statistics and Computing **10** (2000) 197–208
7. Hastings, W.: Monte Carlo sampling methods using Markov chains and their applications. Biometrika **57** (1970) 97–109
8. Luong, Q.T., Faugeras, O.D.: The fundamental matrix: Theory, algorithms, and stability analysis. International Journal of Computer Vision **17** (1996) 43–75
9. Julier, S.J., Uhlmann., J.K.: A new extension of the Kalman filter to nonlinear systems. Int. Symp. Aerospace/Defense Sensing, Simul. and Controls **3** (1997)
10. Bar-Shalom, Y., Li, X.R., Kirubarajan, T.: Estimation with Applications to Tracking and Navigation. John Wiley & Sons, Inc. (2002)
11. Atcheson, B., Heide, F., Heidrich, W.: CALTag: High precision fiducial markers for camera calibration. Vision, Modeling, and Visualization (2010) 41–48